Kinesin-1 structural organization and conformational changes revealed by FRET stoichiometry in live cells

Dawen Cai,[1,2] Adam D. Hoppe,[3] Joel A. Swanson,[3] and Kristen J. Verhey[2]

[1]Biophysics Research Division, [2]Department of Cell and Developmental Biology, and [3]Department of Microbiology and Immunology, University of Michigan, Ann Arbor, MI 48109

Kinesin motor proteins drive the transport of cellular cargoes along microtubule tracks. How motor protein activity is controlled in cells is unresolved, but it is likely coupled to changes in protein conformation and cargo association. By applying the quantitative method fluorescence resonance energy transfer (FRET) stoichiometry to fluorescent protein (FP)–labeled kinesin heavy chain (KHC) and kinesin light chain (KLC) subunits in live cells, we studied the overall structural organization and conformation of Kinesin-1 in the active and inactive states. Inactive Kinesin-1 molecules are folded and autoinhibited such that the KHC tail blocks the initial interaction of the KHC motor with the microtubule. In addition, in the inactive state, the KHC motor domains are pushed apart by the KLC subunit. Thus, FRET stoichiometry reveals conformational changes of a protein complex in live cells. For Kinesin-1, activation requires a global conformational change that separates the KHC motor and tail domains and a local conformational change that moves the KHC motor domains closer together.

Introduction

Long-distance intracellular transport is driven by kinesin and dynein motor proteins that ferry cargoes along microtubule tracks. A large body of work has revealed the chemomechanical mechanisms of motor proteins (Schliwa and Woehlke, 2003; Vale, 2003). However, key aspects of motor-driven transport, such as cargo loading/unloading, regulation of motor activity, and coordination of bidirectional movement, remain unknown.

It has been recognized for some time that motor protein activity must be tightly regulated in cells to prevent the futile hydrolysis of ATP. Current models suggest that only a fraction of Kinesin-1 inside cells is carrying cargo at any time (Hollenbeck, 1989; Verhey et al., 1998). How is Kinesin-1 kept inactive in the absence of cargo? In most species, Kinesin-1 is a heterotetramer of two kinesin heavy chain (KHC) and two kinesin light chain (KLC) polypeptides. Purified Kinesin-1 can exist in two conformations in vitro, depending on ionic concentration, that correlate with the activity of Kinesin-1–folded molecules are thought to be inactive for microtubule-based motility, whereas extended molecules are thought to be active. The folded conformation enables an autoinhibitory interaction of the KHC C-terminal tail with the KHC N-terminal motor (for reviews see Verhey and Rapoport, 2001; Adio et al., 2006). The actin-based motor myosin Va undergoes a similar conformational change that correlates with activity (Liu et al., 2006; Thirumurugan et al., 2006). Thus, autoinhibition may be a general mechanism for the regulation of cytoskeletal motor proteins.

Several lines of evidence suggest that regulation of Kinesin-1 in vivo may be more complex. For example, the motor activity of native, purified Kinesin-1 is typically 10 times less than that of recombinant protein (Hackney et al., 1991; Hancock and Howard, 1998). In addition, the intramolecular association between the N- and C-terminal domains of Kinesin-1 comprises low-affinity interactions in vitro (Stock et al., 1999). Thus, the mechanisms of Kinesin-1 autoinhibition and activation in vivo remain unclear.

To build a structural model of the spatial and molecular relationships within Kinesin-1 in intact cells, we used a quantitative fluorescence resonance energy transfer (FRET) approach (Wallrabe and Periasamy, 2005). We show that FRET stoichiometry (Hoppe et al., 2002), which is a method for measuring both FRET efficiency and the fraction of interacting fluorescent protein (FP) molecules, reveals conformational states of Kinesin-1 in living cells. Specifically, we show that two conformational

Correspondence to Kristen J. Verhey: kjverhey@umich.edu

Abbreviations used in this paper: DTNB, 3-carboxy-4-nitrophenyl disulfide 6,6′-dinitro-3,3′-dithiodibenzoic acid bis(3-carboxy-4-nitrophenyl) disulfide; FP, fluorescent protein; FRET, fluorescence resonance energy transfer; KHC, kinesin heavy chain; KLC, kinesin light chain; mCit, monomeric Citrine; TPR, tetratricopeptide repeat; SLO, streptolysin O.

The online version of this article contains supplemental material.

© The Rockefeller University Press $15.00
The Journal of Cell Biology, Vol. 176, No. 1, January 1, 2007 51–63
http://www.jcb.org/cgi/doi/10.1083/jcb.200605097

changes occur when Kinesin-1 is activated for interaction with microtubule tracks. First, we show for the first time in intact cells that inactive Kinesin-1 is folded in an autoinhibitory conformation, whereas active Kinesin-1 molecules are in a more extended conformation. Second, we describe a novel conformational change in which the two motor domains are pushed apart in the inactive molecule and brought closer together for productive interactions with the microtubules. This novel local conformational change contrasts with what was predicted based on the crystal structure of dimeric Kinesin-1 motors (Kozielski et al., 1997).

Results

FP fusions to KHC and KLC

To analyze the structure of Kinesin-1 in living cells by FRET, donor (monomeric ECFP [mECFP]) and acceptor (monomeric Citrine [mCit]) FPs were fused to the N and/or C termini of both KHC and KLC (Fig. 1 A). COS cells were chosen for their flat morphology and because their low levels of endogenous Kinesin-1 are unlikely to interfere with formation of donor–acceptor FP complexes (Fig. S1 A, available at http://www.jcb.org/cgi/content/full/jcb.200605097/DC1; unpublished data). Only cells expressing low-to-medium levels of FP proteins were chosen for data analysis to avoid artifacts caused by protein aggregation and ATP-independent microtubule interactions (Fig. S1 B). FRET stoichiometry (which is discussed in the following two paragraphs) and coimmunoprecipitation (Fig. S1 A) experiments verified that FP fusions to KHC and KLC did not alter their interactions.

FP-KHC and -KLC expressed in COS cells demonstrated similar localization patterns to those described previously for other tagged Kinesin-1 motors (Fig. S1 B). Because steady-state fluorescence patterns do not indicate the activity of kinesin motors, we developed an assay to delineate between active and inactive motors in vivo. To do this, we took advantage of the ability of the nonhydrolyzable ATP analogue AMPPNP to block the release of active kinesin motors from microtubules (Kawaguchi and Ishiwata, 2001). Live cells were transiently permeabilized with low levels of the bacterial toxin streptolysin O (SLO), and active FP-Kinesin-1 motors were trapped on microtubules by the addition of AMPPNP. FP-Kinesin-1 (e.g., mCit-KHC + HA-KLC; Fig. 1 B, column 1) did not become trapped on microtubules, but remained diffuse and cytosolic upon addition of AMPPNP, indicating that the Kinesin-1 holoenzyme is in an inactive state in vivo. In contrast, in cells expressing FP-KHC

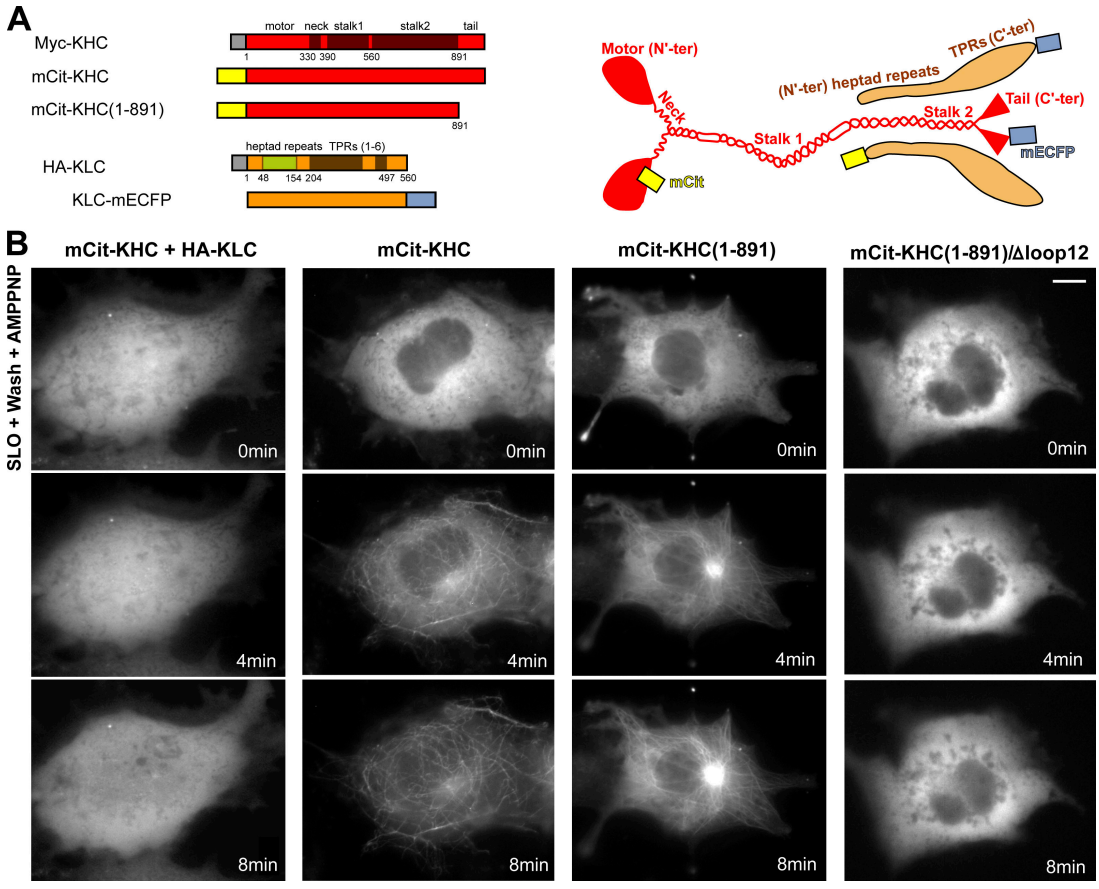

Figure 1. **Localization and activity of FP-tagged Kinesin-1 in COS cells.** (A, left) Schematic diagram of KHC (red) and KLC (orange) domain structure and positions of the epitope and FP tags. (right) Current model of Kinesin-1 structural organization. Red ovals, KHC motor domains; Red triangles, KHC tail domains; yellow rectangles, mCit; cyan rectangles, mECFP. (B) Live-cell microtubule-binding assay. Cells expressing the indicated KHC and/or KLC constructs were transiently permeabilized with SLO, and then AMPPNP was added. Shown is the mCit channel of videos taken during permeabilization (0 min) and the indicated time points after AMPPNP addition. Bar, 10 μm.

alone (e.g., mCit-KHC; Fig. 1 B, column 2), the motor rapidly accumulated on microtubules after exposure to AMPPNP, indicating that the KHC subunit exists in an active state in vivo.

Several lines of evidence verify that FP-KHC alone is capable of ATP-dependent microtubule motility, and thus represents the Kinesin-1 active state. First, single molecule motility assays demonstrate that FP-KHC molecules are capable of microtubule-based motility in vitro (Fig. S1 C). Second, removal of the cryptic ATP-independent microtubule-binding site in the KHC tail (KHC[1–891]) resulted in a KHC molecule that retained ATP-dependent microtubule binding (Fig. 1 B, mCit-KHC[1–891]). Third, this microtubule localization was caused by direct interaction between the KHC motor domain and the microtubules because FRET between mCit-KHC(1–891) and mECFP-tubulin increased after addition of AMPPNP (Fig. S4). Fourth, mutation of the microtubule-binding site in the KHC motor domain (Δloop12 mutation; Woehlke et al., 1997) abolished the ability of FP-KHC to be locked in a microtubule-bound state after addition of AMPPNP (Fig. 1 B, mCit-KHC[1–891]/Δloop12). Collectively, these results indicate that KHC homodimers are active for microtubule binding and motility, whereas the complete Kinesin-1 holoenzyme (KHC + KLC) remains inactive and predominantly in the cytosol. In addition, these results validate the use of fluorophore-tagged subunits to study Kinesin-1 structure and function in vivo.

FRET stoichiometry reveals conformational changes in Kinesin-1 in live cells

For FRET stoichiometry of Kinesin-1, various combinations of KHC and KLC FRET pairs were cotransfected into COS cells, and 24 h later the data were collected on a wide-field fluorescence microscope calibrated for FRET stoichiometry. FRET stoichiometry uses three fluorescence images from a calibrated microscope to calculate three parameters that describe each pixel (Fig. S2, available at http://www.jcb.org/cgi/content/full/jcb.200605097/DC1; Hoppe et al., 2002; Beemiller et al., 2006): (a) R_M, the mole ratio of acceptor- to donor-labeled proteins, (b) E_A, the apparent acceptor FRET efficiency (FRET efficiency × fraction of acceptor molecules in complex), and (c) E_D, the apparent donor FRET efficiency (FRET efficiency × fraction of donor molecules in complex). E_A and E_D range between 0 and 100%, where 100% indicates all acceptor and donor molecules

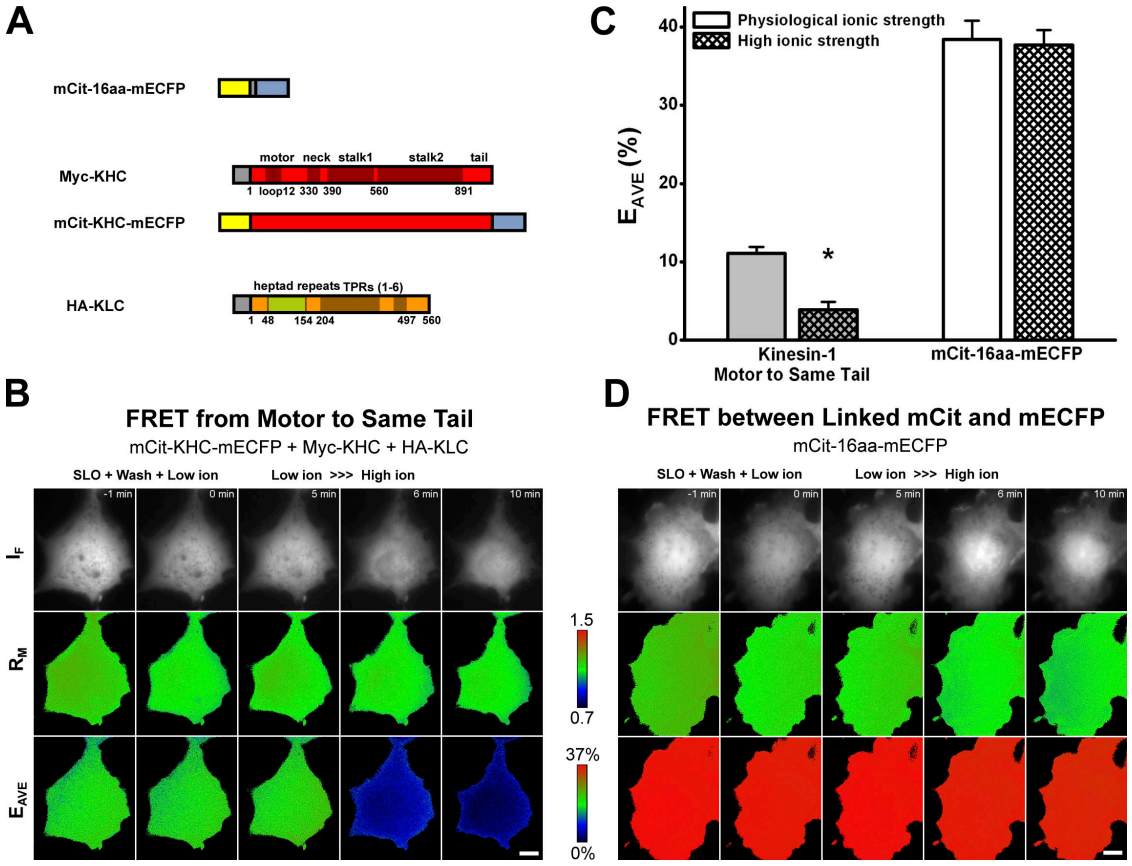

Figure 2. **FRET monitors conformational changes in Kinesin-1 in live cells.** (A) Schematic diagram of the linked mCit-16aa-mECFP calibration molecule, as well as FP-KHC and -KLC constructs. Yellow rectangles, mCit; cyan rectangles, mECFP. (B and D) FRET stoichiometry under different ionic conditions. COS cells expressing mCit-KHC-mECFP + Myc-KHC + HA-KLC (B) or the mCit-16aa-mECFP (D) calibration molecule were imaged (−1 min), permeabilized with SLO (0 min), kept in physiological salt buffer (low ion) for 5 min, and supplemented with high salt (6 min). Shown are the images collected as fluorescence (I_F, top), mCit/mECFP molar ratio (R_M, middle), and FRET efficiency (E_{AVE}, bottom). High salt causes a conformational change in KHC + KLC (B), but not in mCit-16aa-mECFP (D). Bars, 10 μm. (C) Quantification of FRET efficiency for cells expressing mCit-KHC-mECFP + Myc-KHC + HA-KLC (left; $n = 5$) or the mCit-16aa-mECFP molecule (right; $n = 8$) under physiological salt (open bars) and high salt (hatched bars) conditions. Data are the mean ± the SD. *, $P < 0.001$.

in the FRET complex and with complete energy transfer. Because protein expression levels influence the fraction of donor or acceptor molecules in FRET complex for nonlinked molecules, we analyzed cells with R_M close to 1.0 and we calculated an average FRET efficiency, $E_{AVE} = (E_D + E_A)/2$, which is less sensitive to expression ratio (Beemiller et al., 2006). For the control calibration molecule, mECFP-16aa-mCit, $E_{AVE} \approx 37\%$ (Fig. 2 B).

Because the subunits of Kinesin-1 interact with very high affinity and are of known stoichiometry, changes in E_{AVE} should reflect structural changes in the Kinesin-1 molecule. Modeling the spatial arrangements between the FP and the KHC motor domain based on crystal structures supports this assumption, as the short linker sequences (4 or 5 aa) limit the flexibility of the FP (Fig. S1 D). To verify that FRET stoichiometry can detect conformational changes in Kinesin-1 in live cells, we obtained FRET efficiencies under ion concentrations known to induce Kinesin-1 conformational changes in vitro (Hackney et al., 1992). To monitor Kinesin-1 motor-to-tail FRET, FRET pairs were placed on the N and C termini of the same KHC polypeptide (mCit-KHC-mECFP; Fig. 2 A). Coexpression with Myc-KHC was required to prevent aggregation of the four FPs in the KHC homodimer (Fig. S3, available at http://www.jcb.org/cgi/content/full/jcb.200605097/DC1). COS cells expressing mCit-KHC-mECFP + Myc-KHC + HA-KLC (Fig. 2 B) were transiently permeabilized with SLO under physiological salt conditions (I ≈ 0.15). After 5 min, the cells were exchanged into high ionic strength buffer (I ≈ 0.8). High motor-to-tail FRET efficiencies were observed before permeabilization ($E_{AVE} = 11.5 \pm 1.9\%$; Fig. 2 B, E_{AVE}), indicating a close association of the KHC motor and tail regions. FRET remained high during permeabilization at physiological ionic strength (Fig. 2, B [E_{AVE}] and C); however, high ionic strength buffer resulted in a rapid and significant decrease in FRET efficiency ($E_{AVE} = 4.0 \pm 1.1\%$; Fig. 2, B [E_{AVE}] and C). COS cells expressing the mCit-16aa-mECFP calibration molecule exposed to the same conditions showed no significant change in FRET efficiency ($E_{AVE} = 37.8 \pm 2.1\%$ at physiological ionic strength and $37.4 \pm 1.8\%$ at high ionic strength; Fig. 2, C and D [E_{AVE}]). Note that R_M remained constant in both cases, indicating negligible differences in acceptor and donor photobleaching. These results indicate that Kinesin-1 is folded (high motor-to-tail FRET) at physiological ionic strength, but is more extended (low motor-to-tail FRET) under high ionic strength conditions. Thus, FRET stoichiometry can detect conformational changes in Kinesin-1 in living cells.

Structural relationships within inactive Kinesin-1 molecules

To probe the overall structure of inactive Kinesin-1 in vivo, FP-labeled KHC and KLC were coexpressed in COS cells. We first measured FRET efficiencies for FRET pairs located on the KHC subunit (Fig. 3 A, 1–4). For the KHC motor-to-tail relationship, higher FRET efficiencies were obtained for FRET pairs on the same KHC polypeptide ($E_{AVE} = 12.4 \pm 1.0\%$ for mCit-KHC-mECFP + Myc-KHC + HA-KLC; Fig. 3 A, 1) than for FRET pairs on separate KHC polypeptides ($E_{AVE} = 4.8 \pm 0.5\%$ for mCit-KHC + KHC-mECFP + HA-KLC; Fig. 3 A, 2). Although these data cannot distinguish the relationship between each motor and its tail domain because of differences in fraction of FP protein in complex and orientation of the FPs, these FRET efficiencies demonstrate that inactive Kinesin-1 molecules are in a folded conformation in vivo. For KHC motor-to-motor measurements, the FRET efficiency was low ($E_{AVE} = 2.4 \pm 0.5\%$; Fig. 3 A, 3), suggesting that the KHC N-terminal motor domains are separated in the inactive molecule. In contrast, for KHC tail-to-tail measurements, the FRET efficiency was higher ($E_{AVE} = 8.6 \pm 0.9\%$; Fig. 3 A, 4) indicating that the KHC C-terminal tail domains are relatively close together in vivo.

We next measured FRET efficiencies within inactive Kinesin-1 molecules for FRET pairs located on the KLC subunit (Fig. 3 A, 5–7). Little to no FRET was detected between the N and C termini of KLC ($E_{AVE} = 0.2 \pm 0.1\%$; Fig. 3 A, 5), indicating that the KLC subunit is in an extended conformation. Low FRET efficiencies obtained for the C termini of KLC indicate that these regions are separated ($E_{AVE} = 2.3 \pm 0.4\%$; Fig. 3 A, 6), whereas the higher FRET efficiencies obtained for the N termini of KLC indicate that these regions are in close proximity ($E_{AVE} = 11.2 \pm 1.7\%$; Fig. 3 A, 7), presumably because of dimerization via the heptad repeats.

Finally, we measured FRET efficiencies within inactive Kinesin-1 molecules for FRET pairs located on both the KHC and KLC subunits (Fig. 3 A, 8–11). Moderate FRET efficiencies between the C terminus of KLC and either the N terminus of KHC ($E_{AVE} = 5.8 \pm 0.5\%$; Fig. 3 A, 8) or the C terminus of KHC ($E_{AVE} = 6.4 \pm 0.4\%$; Fig. 3 A, 9) suggest that the KLC C terminus is in close proximity to both the KHC motor and tail domains. In contrast, negligible FRET efficiencies were observed between the N terminus of KLC and either the N terminus of KHC ($E_{AVE} = 0.4 \pm 0.1\%$; Fig. 3 A, 10) or the C terminus of KHC ($E_{AVE} = 0.6 \pm 0.3\%$; Fig. 3 A, 11). This suggests that the N terminus of the KLC subunit is close to the region in the KHC stalk that allows folding. These data also indicate that the KLC subunits lie in a direction parallel to the KHC subunits (N' to N' and C' to C'; Fig. 1 A). Collectively, these results support the overall structure of Kinesin-1 gleaned from various in vitro experiments (Vale, 2003) and demonstrate that inactive Kinesin-1 molecules are in a folded conformation in intact cells.

Structural relationships within active Kinesin-1 molecules

To probe the structure of active Kinesin-1 in vivo, we measured FRET efficiencies from combinations of FP-KHCs expressed in COS cells (Fig. 3 B). FRET efficiencies from KHC molecules accumulated at the cell periphery in highly expressed cells (Fig. 3 B, 1–4) were very high ($E_{AVE} > 20\%$), regardless of FP position, and correlated with fluorescence intensities (Fig. S2 C), indicating that intermolecular FRET occurs between crowded KHC molecules accumulated at the plus ends of the microtubules. FRET efficiencies for FP-KHC molecules localized in the rest of the cell (Fig. 3 B, 5–8) remained constant despite variations in fluorescence intensity (Fig. S2 C), suggesting that these FRET measurements represent only intramolecular FRET. Thus, we only collect data from these regions or from

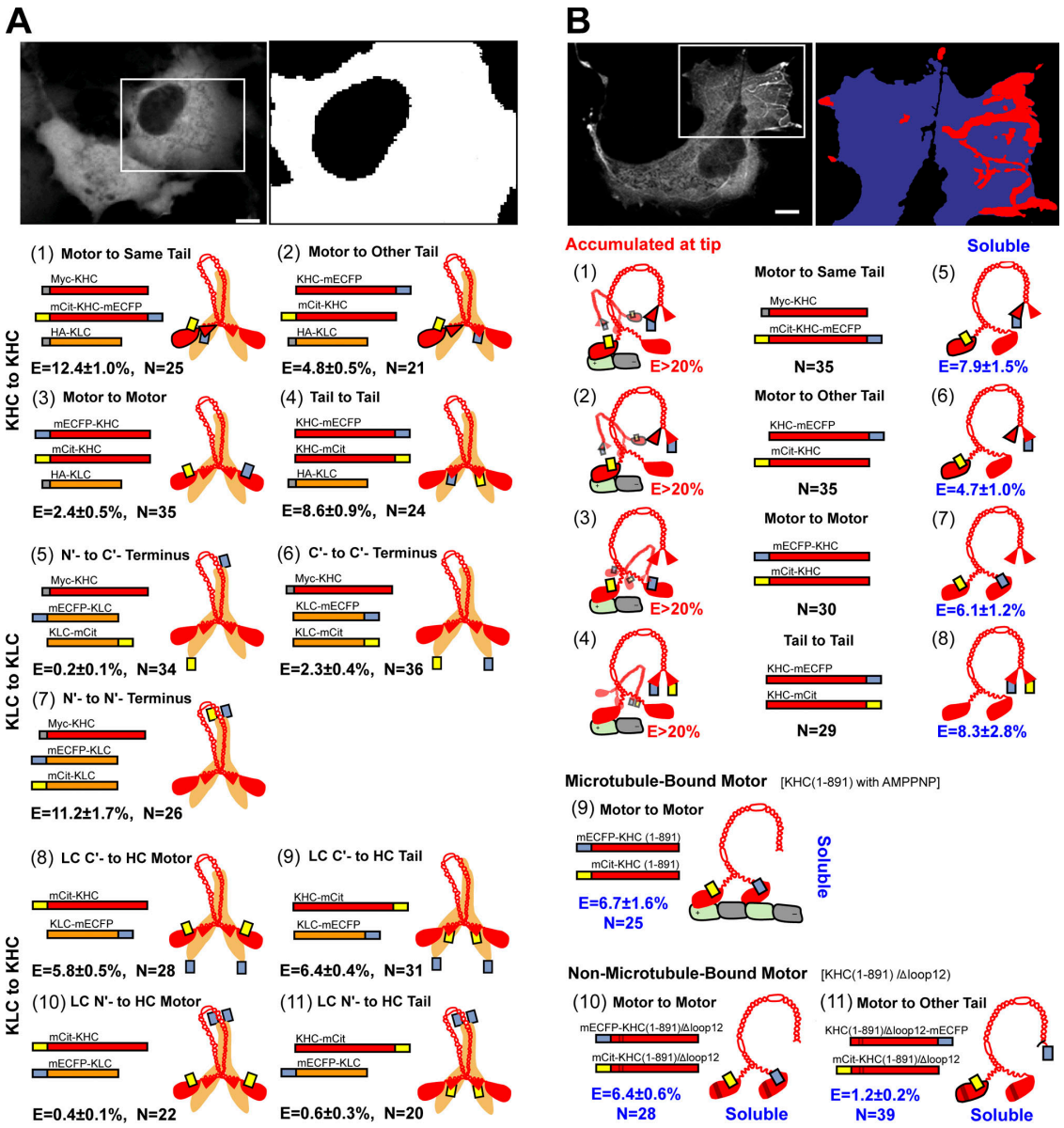

Figure 3. **Structural organization of inactive and active Kinesin-1 in live COS cells.** (A) FRET stoichiometry of inactive Kinesin-1 (KHC + KLC). (top left) Representative fluorescence image. (top right) The white boxed area of the image was enlarged, binned, and threshold-masked for FRET stoichiometry. For 1–11, the FRET pair being analyzed is indicated on the top, the transfected constructs are shown schematically in the middle left, and the calculated FRET efficiencies (E_{AVE}) and *n* values are indicated on the bottom. The cartoon illustration on the right side of each panel indicates the interpreted structure of Kinesin-1 based on the measured FRET efficiencies. In 1 and 2, the black-lined motor and tail domains are from the same KHC polypeptide chain. (B) FRET stoichiometry of active Kinesin-1 (KHC alone). (top left) Representative fluorescence image. (top right) Enlarged, binned, and threshold-masked region for FRET stoichiometry that distinguishes molecules accumulated in the cell periphery (red region in top right and red numbers in 1–4) from molecules soluble in the rest of the cell (blue region in top right and blue numbers in 5–11). For 1–8, the FRET pair being analyzed is indicated at the top, the transfected constructs are shown schematically in the center, and the *n* values are indicated at the bottom. The measured FRET efficiencies and interpreted Kinesin-1 structures are indicated on the left for KHC molecules accumulated at the microtubule plus ends (1–4) and on the right for KHC molecules soluble in the cell (5–8). For 9–11, the data are presented as in A. Microtubules are represented as light green (β-tubulin) and light gray (α-tubulin) rod shapes. "+" and "−" signs represent the plus and minus ends of the microtubules. Yellow rectangles, mCit; cyan rectangles, mECFP. Data are the mean ± the SD. Bars, 10 μm.

cells with low-to-medium expressions to avoid artifacts caused by KHC accumulation.

For KHC motor-to-tail measurements, moderate FRET efficiencies were obtained for FRET pairs on the same KHC polypeptide (E_{AVE} = 7.9 ± 1.5%; Fig. 3 B, 5) and on separate KHC polypeptides (E_{AVE} = 4.7 ± 1.0%; Fig. 3 B, 6), indicating that the motor and tail domains of KHC remain in relatively close proximity upon activation. Moderate FRET efficiencies were also obtained for KHC motor-to-motor FRET pairs (E_{AVE} = 6.1 ± 1.2%; Fig. 3 B, 7) indicating that the two motor domains are in close proximity, as expected for active Kinesin-1. FRET efficiencies obtained for KHC tail-to-tail FRET pairs (E_{AVE} = 8.3 ± 2.8%; Fig. 3 B, 8) indicate that the KHC tails are also in close proximity.

Table I. ***t* test comparing FRET efficiencies of inactive and active Kinesin-1**

Comparison	Expression		E_{AVE}	Fig.	P
			%		
Motor to same tail	Inactive Kinesin-1 (KHC+KLC)	mCit-KHC-mECFP + Myc-KHC + HA-KLC	12.4 ± 1.0	3 A, 1	<0.001
	Active Kinesin-1 (KHC only)	mCit-KHC-mECFP + Myc-KHC	7.9 ± 1.5	3 B, 5	
Motor to other tail	Inactive Kinesin-1 (KHC+KLC)	mCit-KHC + KHC-mECFP + HA-KLC	4.8 ± 0.5	3 A, 2	>0.5
	Active Kinesin-1 (KHC only)	mCit-KHC + KHC-mECFP	4.7 ± 0.1	3 B, 6	
Motor to motor	Inactive Kinesin-1 (KHC+KLC)	mCit-KHC + mECFP-KHC + HA-KLC	2.4 ± 0.5	3 A, 3	<0.001
	Active Kinesin-1 (KHC only)	mCit-KHC + mECFP-KHC	6.1 ± 1.2	3 B, 7	
Tail to tail	Inactive Kinesin-1 (KHC+KLC)	KHC-mCit + KHC-mECFP + HA-KLC	8.6 ± 0.9	3 A, 4	>0.5
	Active Kinesin-1 (KHC only)	KHC-mCit + KHC-mECFP	8.3 ± 2.8	3 B, 8	

To compare the structure of KHC motor domains engaged with microtubules with those in cytosol, FRET efficiencies were measured for KHC molecules forced on or off the microtubules. FP-KHC(1–891) was forced to remain on the microtubule by addition of AMPPNP (Fig. 3 B, 9) or was prevented from binding to microtubules by mutation of the microtubule-binding site in the motor domain (Δloop12 mutation; Fig. 3 B, 10; Woehlke et al., 1997). Similar motor-to-motor FRET efficiencies were obtained for microtubule-bound and unbound motors (E_{AVE} = 6.7 ± 1.6% and 6.4 ± 0.6%, respectively). These results indicate that KHC motor domains in active molecules likely stay in close proximity regardless of whether they are on or off the microtubules.

Two conformational changes in Kinesin-1

To identify conformational changes within Kinesin-1 upon activation, we compared the FRET efficiencies of inactive (KHC + KLC; Fig. 3 A) and active (KHC alone; Fig. 3 B) molecules. KHC motor-to-tail FRET pairs on the same KHC polypeptide had higher FRET efficiency in the presence (E_{AVE} = 12.4 ± 0.1%) than in the absence (E_{AVE} = 7.9 ± 1.5%) of KLC. This difference is statistically significant ($P < 0.001$; Table I) and indicates a smaller distance between the KHC motor and tail domains in the inactive state. This global conformational change (Fig. 4, green arrows) likely displaces the KHC tail from the KHC motor domains for Kinesin-1 activation.

For KHC motor-to-motor FRET pairs, a lower FRET efficiency was observed in the presence (E_{AVE} = 2.4 ± 0.5%) than the absence (E_{AVE} = 6.1 ± 1.2%) of KLC. This difference is statistically significant ($P < 0.001$; Table I) and indicates a larger distance between the two KHC motor domains in the inactive state. That the two KHC motor domains are pushed apart in the inactive holoenzyme was surprising because crystallography and 3D cryoelectron microscopy suggested that the motor domains of truncated KHC molecules are closer together when free in solution than when engaged with a microtubule (Marx et al., 2006). A local conformational change (Fig. 4, blue arrows) upon activation is, thus, likely required to position the motor domains for processive motility.

To confirm that the two KHC motor domains are pushed apart in the inactive state, we tested biochemically whether the KHC neck coiled-coil segments are closer together in the active state (absence of KLC) than in the inactive state (presence of KLC). A Cys residue was introduced into the neck coiled coil of a Cys-lite version of KHC (KHC[Cys344]; Fig. 5 A) at a position accessible to cross-linker, but demonstrated to have no effect on the motile properties of the truncated KHC (Tomishige and Vale, 2000). When COS cell lysates expressing KHC(Cys344) in the absence of KLC (i.e., active Kinesin-1) were treated with the cross-linker 3-carboxy-4-nitrophenyl

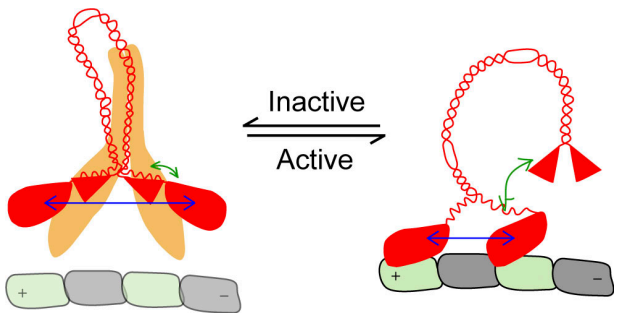

Figure 4. **Conformational changes upon Kinesin-1 activation.** Inactive Kinesin-1 (left) is in a folded conformation such that the KHC motor and tail domains are in close proximity (green arrow), but the KHC motor domains are pushed apart from each other (blue arrow). Upon activation (right), the KHC motor and tail domains are more widely separated (green arrow), whereas the KHC motor domains come closer together (blue arrow). Microtubules are represented as light green (β-tubulin) and light gray (α-tubulin) rod shapes. "+" and "−" signs represent the plus and minus ends of the microtubules.

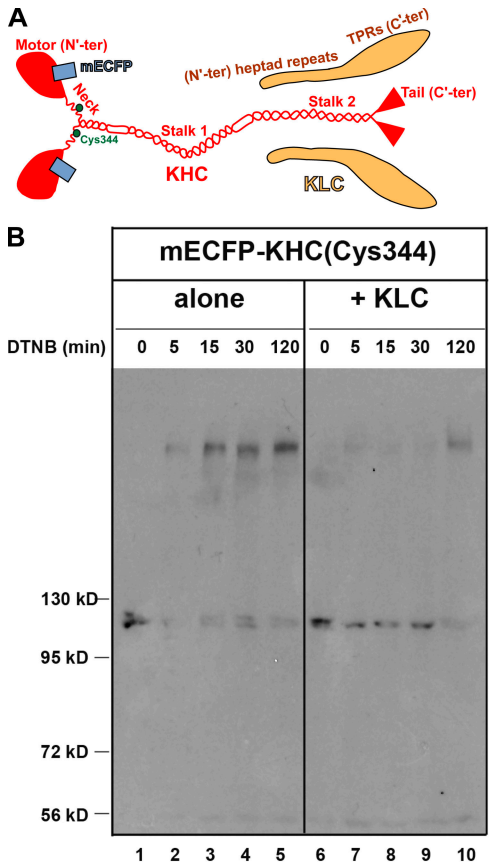

Figure 5. **The KHC motor/neck domains are separated in the inactive molecule by the presence of KLC.** (A) Schematic diagram of mECFP-tagged KHC(Cys344) and KLC in the Kinesin-1 holoenzyme. (B) Lysates of COS cells expressing KHC(Cys344) alone (left) or with KLC (right) were treated with the cross-linker DTNB for the indicated times. Cross-linking was stopped by the addition of SDS-PAGE sample buffer, and the lysates were run on nonreducing SDS PAGE gels, transfered to nitrocellulose, and Western blotted with an antibody to FP tag. The size of molecular weight markers (in kiloDaltons) is indicated on the left of the gel.

disulfide 6,6′-dinitro-3,3′-dithiodibenzoic acid Bis(3-carboxy-4-nitrophenyl) disulfide (DTNB), nearly all of the KHC(Cys344) was rapidly cross-linked as indicated by a shift to a slower mobility form (Fig. 5 B, lanes 2–5). In contrast, in the presence of KLC (i.e., inactive Kinesin-1), little to no cross-linking of KHC(Cys344) was observed (Fig. 5 B, lanes 7–9). Incubation in the presence of DTNB for long periods of time resulted in cross-linking of KHC(Cys344) + KLC (Fig. 5 B, lane 10), presumably caused by "breathing" of the Kinesin-1 holoenzyme. These results confirm that the KHC neck coiled coil is more separated in the inactive state than in the active state.

Contribution of the KHC tail domain to Kinesin-1 autoinhibition

The KHC globular tail domain has been implicated in contributing to both the folded conformation and autoinhibition of KHC in vitro (Coy et al., 1999; Friedman and Vale, 1999; Hackney and Stock, 2000). In particular, a conserved stretch of residues in the KHC tail domain (the IAK region) is critical for autoinhibition of motor activity in vitro (Hackney and Stock, 2000). To determine whether the KHC tail and/or the IAK region play a role in autoinhibition or conformational changes in the Kinesin-1 holoenzyme in vivo, we expressed truncated (KHC[1–891]) and mutated (KHC[ΔIAK]) versions of KHC in COS cells. KHC(1–891) + KLC did not localize to microtubules or accumulate at the cell periphery at steady state, but became locked on microtubules upon exposure of permeabilized cells to AMPPNP (Fig. 6, A [left] and B). The microtubule-bound state of KHC(1–891) + KLC reflects a direct interaction between the motor domain of KHC(1–891) and the microtubule because FRET efficiency between the mCit-KHC(1–891) motor domain and mECFP-tubulin significantly increased upon AMPPNP addition (Fig. S4, available at http://www.jcb.org/cgi/content/full/jcb.200605097/DC1). Like the tail-truncated molecules, Myc-KHC(ΔIAK) + mCit-KLC molecules were capable of microtubule binding (locked on microtubules with AMPPNP; Fig. S5, D and E), but not processive motility (did not accumulate at ends of microtubules; Fig. 6 C). These results indicate that removal of the KHC tail, or mutation of the IAK region, results in a Kinesin-1 holoenzyme that is active for microtubule binding, in contrast to KHC + KLC (Fig. 6, A [right] and B). Thus, the IAK segment of the KHC tail plays an important role in autoinhibition in vivo, specifically in preventing the microtubule association of Kinesin-1.

To test whether activation of Kinesin-1 by mutation of the IAK segment results in a global conformational change in Kinesin-1, we measured motor-to-tail FRET for FRET pairs on the same KHC(ΔIAK) polypeptide (Fig. 6, C–E). High FRET efficiencies were obtained for KHC(ΔIAK) + KLC molecules in the absence of AMPPNP (E_{AVE} = 14.4 ± 1.8%, Fig. 6, C–E), which is similar to wild-type Kinesin-1 (KHC + KLC) molecules with the same labeling (E_{AVE} = 12.4 ± 1.0%; Fig. 3 A, 1), and no change ($P > 0.5$) was detected upon addition of AMPPNP (E_{AVE} = 14.5 ± 2.2%; Fig. 6, C–E). Thus, despite a statistically significant difference ($0.001 < P < 0.01$) in the Relocation Index of KHC(ΔIAK) + KLC (Fig. 6 E, red), no difference in the motor-to-tail spatial relationship (Fig. 6 E, black) was detected ($0.1 < P < 0.5$), even after 30 min of exposure to AMPPNP.

We next looked for a local conformational change in active KHC(ΔIAK) + KLC molecules by measuring motor-to-motor FRET (Fig. 6, F–H). Low FRET efficiencies were obtained in the absence of AMPPNP (E_{AVE} = 2.5 ± 1.5%; Fig. 5, F–H), similar to the values obtained for wild-type Kinesin-1 (E_{AVE} = 2.4 ± 0.5%; Fig. 3 A, 3), and no change ($P > 0.5$) was detected after 10 min of AMPPNP exposure (E_{AVE} = 3.1 ± 0.1%; Fig. 6, F–H). Interestingly, if left in the presence of AMPPNP for 30 min, KHC(ΔIAK) + KLC molecules showed a statistically significant ($P < 0.001$) increase in motor-to-motor FRET (E_{AVE} = 5.7 ± 0.7%; Fig. 6 H, black). This may reflect the ability of Kinesin-1 motors to exist in single- and double-headed binding states in the presence of AMPPNP, with the double-headed state predominating at low load in vitro (Kawaguchi and Ishiwata, 2001) and after prolonged incubation in vivo.

Collectively, these results indicate that the IAK inhibitory region plays an important role in Kinesin-1 autoinhibition in vivo by preventing the microtubule association of inactive Kinesin-1 molecules. The IAK inhibitory region does not, however, contribute to the autoinhibited conformation in vivo

because mutant Kinesin-1 molecules remained tightly folded with the motor domains pushed apart. Thus, other parts of the Kinesin-1 molecule must be required for generating the folded conformation and for keeping the motor domains pushed apart in the absence of cargo.

Contribution of the KLC subunit to Kinesin-1 autoinhibition

The KLC subunit contributes to both the folded conformation of Kinesin-1 and to the separation of the KHC motor domains (Fig. 4). To determine the regions of KLC that contribute to

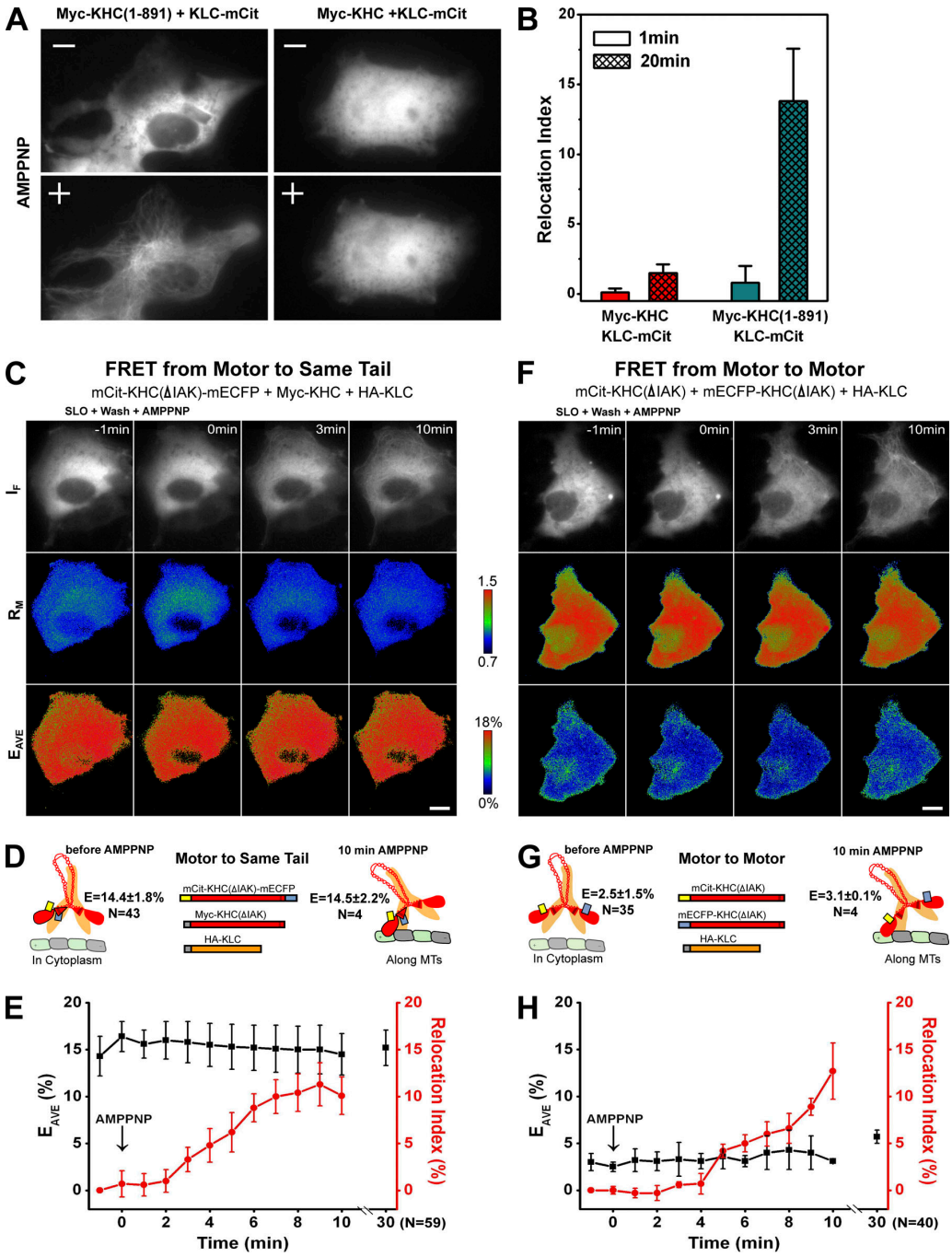

Figure 6. **The KHC tail domain contributes to autoinhibition of Kinesin-1, but not conformational changes.** (A) Live-cell microtubule-binding assay. mCit fluorescence images of COS cells expressing Myc-KHC + KLC-mCit (right) or Myc-KHC(1–891) + KLC-mCit (left) before permeabilization (top) and after 10 min in the presence of AMPPNP (bottom). (B) Quantification of microtubule binding for Myc-KHC + FP-KLC (red bars; $n = 13$) or Myc-KHC(1–891) + FP-KLC (blue bars; $n = 11$) before (open bars) and 20 min after addition of AMPPNP (hatched bars). Motor-to-tail (C–E) and motor-to-motor (F–H) FRET stoichiometry of ΔIAK molecules before and after addition of AMPPNP. (C and F) Shown are the images collected as fluorescence (I_F, top row), ratio (R_M, middle row), and FRET efficiency (E_{AVE}, bottom row). (D and G) FRET pair being analyzed (top center) and schematic of transfected constructs (middle center). Left sides indicate measured FRET efficiencies, *n* values, and illustration of interpreted FRET results before the addition of AMPPNP, whereas the right sides indicate the same for after addition of AMPPNP. (E and H) Time course of change in FRET efficiency (E_{AVE}, black line) and Relocation Index (red line). Data are the mean ± the SD. Bars, 10 μm.

autoinhibition in vivo, we used a truncated version of KLC (KLC[1–176]) that lacks the tetratricopeptide repeat (TPR) motifs required for cargo binding, but retains the heptad repeats required for association with KHC (Verhey et al., 1998). FP-KHC + FP-KLC(1–176) localized to the cytosol at steady-state and after exposure of cells to AMPPNP, similar to wild-type Kinesin-1 (Fig. S5, D and E), indicating that the heptad repeat region of KLC is sufficient for autoinhibition. This is likely caused by the ability of the KLC heptad repeats to maintain the folded conformation (Fig. 7 B, top), as no statistically significant difference was seen ($0.1 < P < 0.5$) in the motor-to-tail FRET efficiency of mCit-KHC-mECFP + KLC(1–176) (E_{AVE} = 12.1 ± 0.7%; Fig. 7 A, 2) when compared with that of wild-type Kinesin-1 (mCit-KHC-mECFP + KLC, E_{AVE} = 12.4 ± 1.0%; Fig. 7 A, 1).

We next looked for a local conformational change in KHC + KLC(1–176) molecules by measuring KHC motor-to-motor FRET (Fig. 7 A, 3–6). Significantly higher FRET efficiencies ($P < 0.001$) were obtained for FP-KHC + KLC(1–176) (E_{AVE} = 5.3 ± 0.5%; Fig. 7 A, 4) than for wild-type Kinesin-1 (E_{AVE} = 2.4 ± 0.5%; Fig. 7 A, 3), indicating that the KHC motor domains are closer together when the KLC TPR motifs are removed (Fig. 7 B, bottom). To test whether the KHC tail domains also play a role in separating the motor domains, we compared the motor-to-motor relationships of molecules containing truncations of KLC, KHC, or both. KHC motors that are incapable of binding to microtubules (KHC[1–891]/Δloop 12 mutant) were used to eliminate potential effects that microtubule binding may have on motor-to-motor distances. Truncation of the KHC tail domain (KHC[1–891]/Δloop12 + KLC) caused no significant change ($P > 0.5$) in motor-to-motor FRET when compared with wild-type Kinesin-1 molecules (KHC + KLC; E_{AVE} = 2.3 ± 0.8%; Fig. 7 A, 5, vs. E_{AVE} = 2.4 ± 0.5%; Fig. 7 A, 3, respectively) and a small increase ($0.01 < P < 0.02$) in motor-to-motor FRET when compared with KLC-truncated Kinesin-1 molecules (E_{AVE} = 6.2 ± 1.9%; Fig. 7 A, 6 vs. E_{AVE} = 5.3 ± 0.5%; Fig. 7 A, 4). In contrast, truncation of KLC caused a significant change ($P < 0.001$) in motor-to-motor FRET when compared with either wild-type Kinesin-1 molecules (E_{AVE} = 5.3 ± 0.5%; Fig. 7 A, 4 vs. E_{AVE} = 2.4 ± 0.5%; Fig. 7 A, 3, respectively) or to KHC-truncated Kinesin-1 molecules (E_{AVE} = 6.2 ± 1.9%; Fig. 7 A, 6 vs. E_{AVE} = 2.3 ± 0.8%; Fig. 7 A, 5, respectively). These results indicate that the major contribution for separation of the KHC motor domains in the inactive conformation is provided by the KLC TPR motifs.

Discussion

Knowledge of the structural organization of Kinesin-1 is essential to understanding how it interacts with cargo components, how it generates motile force, and how motility is controlled. In this report, we demonstrate the feasibility of using FRET stoichiometry to determine the domain orientations and spatial relationships of Kinesin-1 in living cells. This approach is particularly beneficial for studying protein complexes where recombinant expression may not reflect the true folding, subunit interactions, and/or posttranslational modifications of a multiprotein complex.

Advantages of FRET stoichiometry

FRET methods have been successfully used to investigate protein interactions and conformational changes of individual

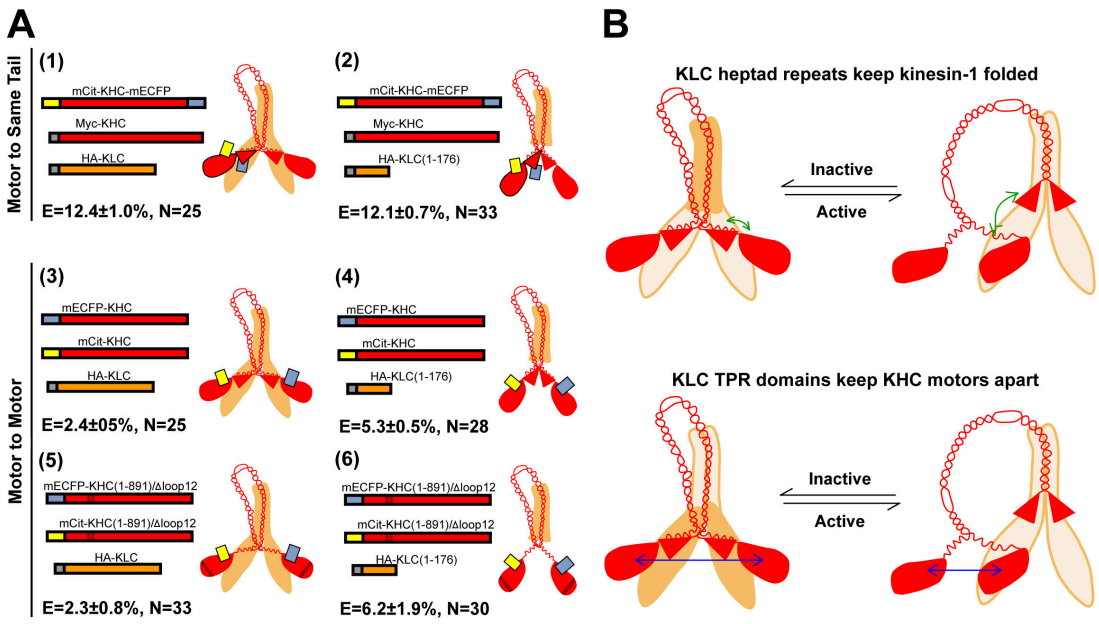

Figure 7. **The KLC subunit contributes to both autoinhibition and conformational changes.** (A, 1–6) The FRET pair being analyzed is indicated vertically to the left of the panels, the transfected constructs are shown schematically in the middle left, and the calculated FRET efficiencies (E_{AVE}) and *n* values are indicated on the bottom left. The cartoon illustration on the right side of each panel indicates the interpreted structure of Kinesin-1, based on the measured FRET efficiencies. In 1 and 2, the black-lined motor and tail domains are from the same KHC polypeptide chain. (B) Model for how KLC domains contribute to autoinhibition of Kinesin-1. In the absence of the TPR motifs, the heptad repeats contribute to autoinhibition by promoting the folded conformation (green arrows, top). The TPR motifs contribute to autoinhibition by separating the KHC motor domains (blue arrows, bottom). Data are the mean ± the SD.

proteins inside cells (Wallrabe and Periasamy, 2005). We show that FRET stoichiometry reveals structural organization and conformational changes of a molecular complex. FRET stoichiometry is a superior method for in vivo analysis because it quantifies fundamental parameters describing both proteins interactions and the FRET efficiency (i.e., R_M, E_A, and E_D). Other FRET approaches, such as acceptor photobleaching, provide only E_D and do not account for modulation of FRET signals by protein expression ratios. These methods may also be complicated by photoconversion of CFP to a YFP-like chromophore under high laser illumination (Valentin et al., 2005). Other multispectral FRET approaches have been developed (Gordon et al., 1998); however, these calculate arbitrary and nonlinear indicators of FRET, and therefore cannot interpret structural changes in a molecule. Furthermore, FRET stoichiometry is linear and does not require fluorescence lifetime, contrary to some confusion in the literature (Zal and Gascoigne, 2004).

FRET efficiency reflects the distance and orientation between the FP tags. E_{AVE} could thus be used to compute distances between donor and acceptor in these complexes from the usual equation:

$$E = R_0^6 \Big/ \left(r^6 + R_0^6\right),$$

where R_0 is the Förster distance. However, the complications associated with expression ratio and slow rotational fluorophore diffusion invalidate the assumption that $\kappa^2 = 2/3$ and permit only rough distance calculations. For example, the distance between the N termini of dimeric KHC motors bound to the microtubule should be less than the distance between two adjacent β-tubulin subunits (~8 nm; Hoenger et al., 2000). We measured motor-to-motor FRET of KHC(1–891) bound to microtubules with AMPPNP in vivo ($E_{AVE} = 6.7 \pm 1.6\%$; Fig. 3 B, 9). Multiplied by 2 to account for random pairing of donor and acceptors, this value ($E_{AVE} = 13.4\%$) corresponds to a distance of ~6.8 nm, with the assumption that $R_0 \approx 50$ Å (Tsien, 1998). Taking into account the fact that FRET measurements reflect the distance between the chromophoric centers of the FPs, rather than the actual distance between the KHC N termini, these results demonstrate that the FRET measurements obtained in this study are comparable to known structural measurements.

Autoinhibition of Kinesin-1

Our FRET stoichiometry results support current models of the organization of KHC and KLC polypeptides in the Kinesin-1 holoenzyme (Vale, 2003). In addition, our results extend previous in vitro analyses by demonstrating that inactive Kinesin-1 molecules exist in a folded conformation in vivo. Folding of Kinesin-1 is likely caused by helix-breaking residues in the KHC stalk domain. Although mutation of hinge2 in KHC resulted in higher ATPase and microtubule motility activities, velocity sedimentation analysis indicated a folded conformation (Coy et al., 1999; Friedman and Vale, 1999). Thus, it will be interesting to probe the folded state of Δhinge molecules by FRET stoichiometry.

Our results demonstrate that two regions of Kinesin-1 are required to keep the motor autoinhibited in the absence of cargo. First, the IAK region of the KHC tail prevents the initial binding of the KHC motor domain to the microtubule. These results extend the original in vitro observations (Hackney and Stock, 2000) by demonstrating that the IAK region is necessary for autoinhibition (a) in the Kinesin-1 holoenzyme and (b) in vivo. The IAK region is not, however, sufficient for autoinhibition under physiological conditions because full-length KHC molecules (i.e., lacking KLC) are capable of microtubule binding and motility. This is likely caused by the inability of weak KHC neck-to-tail interactions (Bathe et al., 2005; Stock et al., 1999) to maintain the tightly folded conformation.

Second, the TPR motifs of the KLC subunit push the KHC motors apart in the inactive conformation. This novel "heads apart" inactive state was surprising because crystallographic and cryoelectron microscopic studies showed that the Kinesin-1 motor domains are closer together in solution (inactive state) than when docked on a microtubule protofilament (active sate; Marx et al., 2006). A separation of the KHC motor domains was likely missed in previous studies that analyzed truncated forms of KHC in the absence of KLC. Although the original premise that unwinding of the neck coiled coil is required for processive motility has been disproved, we suggest that that unwinding of the Kinesin-1 neck coiled coil is required for autoinhibition, specifically to separate the KHC motor domains and prevent processive motility. This model can explain why several non-ideal coiled-coil residues in the neck have been so highly conserved (Bathe et al., 2005; Adio et al., 2006; Marx et al., 2006). In addition, our results fit well with a recent model put forth for *Neurospora crassa* KHC in which an interaction with the KHC tail domain leads to a non–coiled-coil conformation of the neck (Bathe et al., 2005). These results underscore the importance of KLC in regulation of Kinesin-1 activity in vivo (Hackney et al., 1991; Gindhart et al., 1998; Verhey et al., 1998; Martin et al., 1999; Rahman et al., 1999). In cases where KLC subunits have either not been found (e.g., *N. crassa*; Adio et al., 2006) or are not essential for specific transport events (Palacios and St Johnston, 2002; Ling et al., 2004), how KHC activity is regulated remains to be determined.

Activation of Kinesin-1 requires two conformational changes

A comparison of the spatial relationships within Kinesin-1 reveals two conformational changes that occur upon motor activation. First, a novel local conformational change brings the two KHC motor domains closer together, presumably in proper position for processive motility (Fig. 4, green arrows). Second, a global conformational change separates the KHC motor and tail domains, freeing the motor domains for microtubule binding (Fig. 4, blue arrows). Interestingly, in the active state, FRET efficiencies between the KHC N-terminal motor and C-terminal tail are >0%. This suggests that the linear depiction of Kinesin-1 based on cryoelectron microscopy (80 nm from motor-to-tail) is an artifact of those experimental conditions (Hisanaga et al., 1989). Rather, Kinesin-1 is likely to be partially folded while undergoing microtubule-based transport (Hisanaga et al., 1989; Verhey et al., 1998; Coy et al., 1999; Friedman and Vale, 1999). Additional work is needed to understand the spatial relationships in cargo-bound Kinesin-1 molecules.

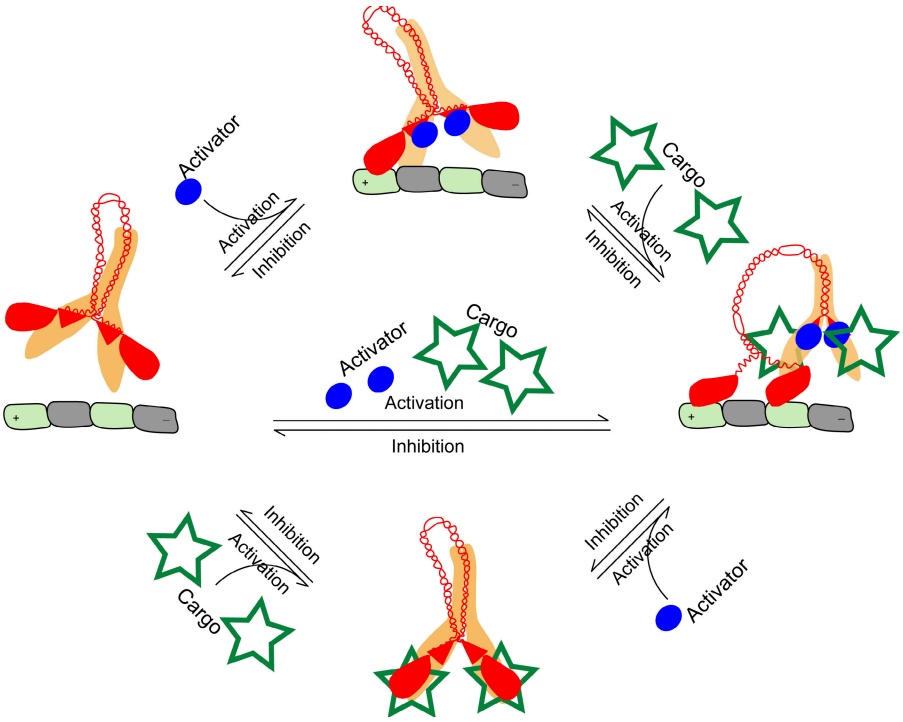

Figure 8. **Model for activation of Kinesin-1.** Full activation of Kinesin-1 requires that the inhibitory effects of both the KHC tail and the KLC subunit must be relieved. This likely requires both cargo (green stars) binding to the KLC TPRs (shown) and cargo or activator (blue ovals) binding to the KHC tail. These two processes may act sequentially (top and bottom paths) or in concert (middle path). Microtubules are represented as light green (β-tubulin) and light gray (α-tubulin) rod shapes. "+" and "−" signs represent the plus and minus ends of the microtubules.

How autoinhibition is relieved is unknown, but must involve conformational changes that separate the inhibitory and enzymatic domains. Full activation of Kinesin-1 for microtubule-based motility requires that the inhibitory effects of both the KHC tail and the KLC subunit be relieved to achieve these two conformational changes (Fig. 8). Recent data from our lab (Blasius et al., 2007) demonstrates that binding of the Kinesin-1 cargo protein JNK-interacting protein 1 to the KLC subunit is not sufficient to activate Kinesin-1. Similarly, binding of fasciculation and elongation factor 1 to the KHC tail is not sufficient for motor activation. Only when binding partners of both the KLC subunit and the KHC tail (JNK-interacting protein 1 and fasciculation and elongation factor 1, respectively) are present is Kinesin-1 activated for microtubule binding and motility.

Autoinhibition as a control mechanism

Defining the mechanisms of inhibition and elucidating how inhibition is relieved is key to understanding biological regulatory strategies. Autoinhibition of Kinesin-1 prevents futile ATP hydrolysis and allows rapid and specific control of motor activity both temporally and spatially. Autoinhibition of Kinesin-1 requires surprisingly small regions of the protein involved in weak intramolecular interactions. Flexibility of the molecule is, thus, essential to bringing the interacting segments into close molecular contact, thereby generating relatively high effective local concentrations.

Autoinhibition is a common regulatory strategy used in diverse biological systems (Pufall and Graves, 2002; Schlessinger, 2003). Notably, autoinhibition mechanisms have been proposed for members of both the kinesin (Lee et al., 2004; Imanishi et al., 2006) and myosin families (Liu et al., 2006; Thirumurugan et al., 2006), as well as proteins that control the polymerization dynamics of both the actin and microtubule cytoskeletons, such as Wiscott-Aldrich Syndrome protein (Millard et al., 2004), mDia/formins (Higgs, 2005), and cytoplasmic linker protein 170 (Lansbergen et al., 2004). Such a regulatory mechanism is fitting for cytoskeletal systems that undergo rapid dynamics to drive a wide variety of cellular functions. It will be interesting to find out how autoinhibition regulates other motors

Materials and methods

Plasmids

Myc-tagged rat KHC and KHC(1–891), as well as HA-tagged rat KLC and KLC(1–176), have been previously described (Verhey et al., 1998). Monomeric versions of the FPs ECFP (mECFP) and mCit (an EYFP variant that is a superior acceptor for FRET; Griesbeck et al., 2001; Hoppe et al., 2002) were used to minimize dimerization artifacts. All FP-KHC and FP-KLC fusion proteins were created in the mECFP-C1, mECFP-N1, mCit-C1, and mCit-N1 vectors (CLONTECH Laboratories, Inc.) by PCR using primers with appropriate restriction sites and verified by DNA sequencing.

A 4-aa linker (SGAG) was inserted between the FP and KHC or KLC in the FP-C1 vectors (e.g., mCit-4aa-KHC). A 5-aa linker (GPVAT) was inserted between KHC or KLC and the FP in FP-N1 vectors (e.g., KHC-5aa-mECFP), whereas a 10-aa linker (GAGTGGGGGT) was used for KHC constructs tagged with both mCit and mECFP molecules (e.g., mCit-4aa-KHC-10aa-mECFP). The KLC-mECFP and KLC-mCit constructs also contain an HA tag at the N terminus (e.g., HA-KLC-mECFP) that is not indicated in the text or figures for clarity (Fig. S1). The HA tag was not used for linking the FP and KLC, but rather for ease of cloning. ECFP-tubulin was from CLONTECH Laboratories, Inc. The linked mCit-16aa-mECFP calibration molecule has been previously described (Hoppe et al., 2002).

Mutation of loop 12 (Δloop12: H275, R279, and K282 to Ala; Woehlke et al., 1997) and the IAK region (ΔIAK: Q920, I921, A922, K923, P924, I925, R926, P927, and G928 to Ala) within the full-length rat KHC sequence was done by overlapping PCR. KHC(Cys344) was created by first fusing a Cys-lite version of human KHC(1–560) containing the introduced Cys344 (HK560[Cys344], a gift from R. Vale [University of California, San Francisco, San Francisco, CA]; Tomishige and Vale, 2000) to rat KHC(556–955) by overlapping PCR. Cys628 in rat KHC was then mutated to Ser by PCR.

Cell culture, permeabilization, and cross-linking

COS cells were cultured as previously described (Verhey et al., 1998), except that TransIT-LTI (Mirus) was used for transfection. A coverglass with

transfected cells was assembled in a Leiden's chamber and maintained at 37°C in Ringer's buffer (10 mM Hepes, 155 mM NaCl, 5 mM KCl, 2 mM $CaCl_2$, 1 mM $MgCl_2$, 2 mM NaH_2PO_4, and 10 mM glucose, pH 7.2). 0.1 μg/ml SLO (in Ringer's buffer with 10 mg/ml of BSA) was added for 30 s, the cells were rapidly washed three times with Buffer I (25 mM Hepes, 5 mM $MgCl_2$, 115 mM KOAc, 5 mM NaOAc, 0.5 mM EGTA, pH 7.2, and 10 mg/ml of BSA), and 1 mM of AMPPNP or 625 mM NaCl was added.

COS cells expressing KHC(Cys344) in the absence and presence of KLC were lysed in lysis buffer (25 mM Hepes/KOH, 5 mM $MgCl_2$, 115 mM KOAc, 5 mM NaOAc, and 0.5 mM EGTA, pH 7.2) at 4°C and cleared by centrifugation. Lysates were or were not incubated with 200 μM DTNB at 4°C for various times. The reaction was stopped by addition of SDS sample buffer. Proteins were separated on 6% SDS-PAGE gel and immunoblotted with a polyclonal antibody to the FP (Invitrogen).

Fluorescence microscopy

Fluorescence images were acquired using an inverted microscope (Eclipse TE-300; Nikon) with a 60×, NA 1.4, oil-immersion PlanApo objective lens (Nikon) and Lambda LS Xenon arc lamp (Sutter Instruments). Image acquisition was controlled by Metamorph 6.2r6 (Universal Imaging). Fluorescence excitation and emission wavelengths were selected using an 86006 filter set (Chroma Technology) and Lambda 10–2 filter wheel controller (Sutter Instruments) equipped with a shutter for epifluorescence illumination control. Images were acquired by a Photometrics Quantix cooled charge-coupled device camera (Roper Scientific) with exposure times of 100–800 ms. All microscopy was carried out at 37°C.

FRET stoichiometry, data processing, data sampling, and statistical analysis

All images used for FRET microscopy were corrected for illumination shading and bias offset by collecting shade images from a mixture of mECFP and mCit sandwiched between two coverslips, and by collecting bias images with the excitation light blocked. The FRET microscope was calibrated to obtain the parameters α, β, γ, and ξ from COS7 cells expressing mCit (α), mECFP (β), or a mECFP-mCit molecule linked by 16 aa (γ and ξ) whose FRET efficiency (E) was measured by fluorescence lifetime spectroscopy (Hoppe et al., 2002). Calculation of E_A, E_D, E_{AVE}, and R_M images was performed using the corrected fluorescence images and FRET parameters as previously described (Beemiller et al., 2006). These equations are identical to those described previously (Hoppe et al., 2002), except that the ratio of γ/ξ was replaced with simply ξ. Using ImageJ (National Institutes of Health), a binary mask was generated on the I_F image and applied to the E_{AVE} and R_M images. For highly expressing cells only, a measurement region that excluded the nucleus and FP-molecules accumulated at the cell periphery (Fig. S2) was defined and used to record the average pixel values for each cell from the E_{AVE} and R_M images. A two-tailed *t* test was used to compare steady-state E_{AVE} values. The Relocation Index is described in Fig. S5. For comparing time-lapse FRET or Relocation Index changes, a paired two-tailed *t* test was used.

Online supplemental material

Fig. S1 shows that FP fusions to KHC and KLC do not affect the interactions or activities of the Kinesin-1 subunits. Fig. S2 shows the equations and methods of FRET stoichiometry. Fig. S3 shows measurements of KHC motor-to-same tail FRET requires coexpression of mCit-KHC-mECFP with Myc-KHC. Fig. S4 shows microtubule localization of active Kinesin-1 molecules results in FRET between Kinesin-1 and tubulin. Fig. S5 shows that the KLC heptad repeats are sufficient for autoinhibition of Kinesin-1. Online supplemental material is available at http://www.jcb.org/cgi/content/full/jcb.200605097/DC1.

We thank E. Meyhofer of the University of Michigan for the use of the Total Internal Reflection Fluorescent microscope and help with in vitro motility assays and R. Vale for the Cys-lite KHC(1-560) construct.

This work was supported by grants from the National Institutes of Health to K.J. Verhey (GM070862) and J.A. Swanson (AI64668).

Submitted: 16 May 2006
Accepted: 1 December 2006

References

Adio, S., J. Reth, F. Bathe, and G. Woehlke. 2006. Review: regulation mechanisms of Kinesin-1. *J. Muscle Res. Cell Motil.* 27:153–160.

Bathe, F., K. Hahlen, R. Dombi, L. Driller, M. Schliwa, and G. Woehlke. 2005. The complex interplay between the neck and hinge domains in kinesin-1 dimerization and motor activity. *Mol. Biol. Cell*. 16:3529–3537.

Beemiller, P., A.D. Hoppe, and J.A. Swanson. 2006. A phosphatidylinositol-3-kinase-dependent signal transition regulates ARF1 and ARF6 during Fcgamma receptor-mediated phagocytosis. *PLoS Biol.* 4:e162.

Blasius, T.L., D. Cai, G.T. Jih, C.P. Toret, and K.J. Verhey. 2007. Two binding partners cooperate to activate the molecular motor Kinesin-1. *J. Cell Biol.* 176:11–17.

Coy, D.L., W.O. Hancock, M. Wagenbach, and J. Howard. 1999. Kinesin's tail domain is an inhibitory regulator of the motor domain. *Nat. Cell Biol.* 1:288–292.

Friedman, D.S., and R.D. Vale. 1999. Single-molecule analysis of kinesin motility reveals regulation by the cargo-binding tail domain. *Nat. Cell Biol.* 1:293–297.

Gindhart, J.G., Jr., C.J. Desai, S. Beushausen, K. Zinn, and L.S. Goldstein. 1998. Kinesin light chains are essential for axonal transport in *Drosophila*. *J. Cell Biol.* 141:443–454.

Gordon, G.W., G. Berry, X.H. Liang, B. Levine, and B. Herman. 1998. Quantitative fluorescence resonance energy transfer measurements using fluorescence microscopy. *Biophys. J.* 74:2702–2713.

Griesbeck, O., G.S. Baird, R.E. Campbell, D.A. Zacharias, and R.Y. Tsien. 2001. Reducing the environmental sensitivity of yellow fluorescent protein. Mechanism and applications. *J. Biol. Chem.* 276:29188–29194.

Hackney, D.D., and M.F. Stock. 2000. Kinesin's IAK tail domain inhibits initial microtubule-stimulated ADP release. *Nat. Cell Biol.* 2:257–260.

Hackney, D.D., J.D. Levitt, and D.D. Wagner. 1991. Characterization of alpha 2 beta 2 and alpha 2 forms of kinesin. *Biochem. Biophys. Res. Commun.* 174:810–815.

Hackney, D.D., J.D. Levitt, and J. Suhan. 1992. Kinesin undergoes a 9 S to 6 S conformational transition. *J. Biol. Chem.* 267:8696–8701.

Hancock, W.O., and J. Howard. 1998. Processivity of the motor protein kinesin requires two heads. *J. Cell Biol.* 140:1395–1405.

Higgs, H.N. 2005. Formin proteins: a domain-based approach. *Trends Biochem. Sci.* 30:342–353.

Hisanaga, S., H. Murofushi, K. Okuhara, R. Sato, Y. Masuda, H. Sakai, and N. Hirokawa. 1989. The molecular structure of adrenal medulla kinesin. *Cell Motil. Cytoskeleton*. 12:264–272.

Hoenger, A., M. Thormahlen, R. Diaz-Avalos, M. Doerhoefer, K.N. Goldie, J. Muller, and E. Mandelkow. 2000. A new look at the microtubule binding patterns of dimeric kinesins. *J. Mol. Biol.* 297:1087–1103.

Hollenbeck, P.J. 1989. The distribution, abundance and subcellular localization of kinesin. *J. Cell Biol.* 108:2335–2342.

Hoppe, A., K. Christensen, and J.A. Swanson. 2002. Fluorescence resonance energy transfer-based stoichiometry in living cells. *Biophys. J.* 83:3652–3664.

Imanishi, M., N.F. Endres, A. Gennerich, and R.D. Vale. 2006. Autoinhibition regulates the motility of the *C. elegans* intraflagellar transport motor OSM-3. *J. Cell Biol.* 174:931–937.

Kawaguchi, K., and S. Ishiwata. 2001. Nucleotide-dependent single- to double-headed binding of kinesin. *Science*. 291:667–669.

Kozielski, F., S. Sack, A. Marx, M. Thormahlen, E. Schonbrunn, V. Biou, A. Thompson, E.M. Mandelkow, and E. Mandelkow. 1997. The crystal structure of dimeric kinesin and implications for microtubule-dependent motility. *Cell*. 91:985–994.

Lansbergen, G., Y. Komarova, M. Modesti, C. Wyman, C.C. Hoogenraad, H.V. Goodson, R.P. Lemaitre, D.N. Drechsel, E. van Munster, T.W. Gadella Jr., et al. 2004. Conformational changes in CLIP-170 regulate its binding to microtubules and dynactin localization. *J. Cell Biol.* 166:1003–1014.

Lee, J.R., H. Shin, J. Choi, J. Ko, S. Kim, H.W. Lee, K. Kim, S.H. Rho, J.H. Lee, H.E. Song, et al. 2004. An intramolecular interaction between the FHA domain and a coiled coil negatively regulates the kinesin motor KIF1A. *EMBO J.* 23:1506–1515.

Ling, S.C., P.S. Fahrner, W.T. Greenough, and V.I. Gelfand. 2004. Transport of *Drosophila* fragile X mental retardation protein-containing ribonucleoprotein granules by kinesin-1 and cytoplasmic dynein. *Proc. Natl. Acad. Sci. USA*. 101:17428–17433.

Liu, J., D.W. Taylor, E.B. Krementsova, K.M. Trybus, and K.A. Taylor. 2006. Three-dimensional structure of the myosin V inhibited state by cryoelectron tomography. *Nature*. 442:208–211.

Martin, M., S.J. Iyadurai, A. Gassman, J.G. Gindhart Jr., T.S. Hays, and W.M. Saxton. 1999. Cytoplasmic dynein, the dynactin complex, and kinesin are interdependent and essential for fast axonal transport. *Mol. Biol. Cell*. 10:3717–3728.

Marx, A., J. Muller, E.M. Mandelkow, A. Hoenger, and E. Mandelkow. 2006. Interaction of kinesin motors, microtubules, and MAPs. *J. Muscle Res. Cell Motil.* 27:125–137.

Millard, T.H., S.J. Sharp, and L.M. Machesky. 2004. Signalling to actin assembly via the WASP (Wiskott-Aldrich syndrome protein)-family proteins and the Arp2/3 complex. *Biochem. J.* 380:1–17.

Palacios, I.M., and D. St Johnston. 2002. Kinesin light chain-independent function of the Kinesin heavy chain in cytoplasmic streaming and posterior localisation in the *Drosophila* oocyte. *Development*. 129:5473–5485.

Pufall, M.A., and B.J. Graves. 2002. Autoinhibitory Domains: modular effectors of cellular regulation. *Annu. Rev. Cell Dev. Biol.* 18:421–462.

Rahman, A., A. Kamal, E.A. Roberts, and L.S. Goldstein. 1999. Defective kinesin heavy chain behavior in mouse kinesin light chain mutants. *J. Cell Biol.* 146:1277–1288.

Schlessinger, J. 2003. Signal transduction. Autoinhibition control. *Science*. 300:750–752.

Schliwa, M., and G. Woehlke. 2003. Molecular motors. *Nature*. 422:759–765.

Stock, M.F., J. Guerrero, B. Cobb, C.T. Eggers, T.G. Huang, X. Li, and D.D. Hackney. 1999. Formation of the compact confomer of kinesin requires a COOH-terminal heavy chain domain and inhibits microtubule-stimulated ATPase activity. *J. Biol. Chem.* 274:14617–14623.

Thirumurugan, K., T. Sakamoto, J.A. Hammer III, J.R. Sellers, and P.J. Knight. 2006. The cargo-binding domain regulates structure and activity of myosin 5. *Nature*. 442:212–215.

Tomishige, M., and R.D. Vale. 2000. Controlling kinesin by reversible disulfide cross-linking: identifying the motility-producing conformational change. *J. Cell Biol.* 151:1081–1092.

Tsien, R.Y. 1998. The green fluorescent protein. *Annu. Rev. Biochem.* 67:509–544.

Vale, R.D. 2003. The molecular motor toolbox for intracellular transport. *Cell*. 112:467–480.

Valentin, G., C. Verheggen, T. Piolot, H. Neel, M. Coppey-Moisan, and E. Bertrand. 2005. Photoconversion of YFP into a CFP-like species during acceptor photobleaching FRET experiments. *Nat. Methods*. 2:801.

Verhey, K.J., and T.A. Rapoport. 2001. Kinesin carries the signal. *Trends Biochem. Sci.* 26:545–550.

Verhey, K.J., D.L. Lizotte, T. Abramson, L. Barenboim, B.J. Schnapp, and T.A. Rapoport. 1998. Light chain–dependent regulation of kinesin's interaction with microtubules. *J. Cell Biol.* 143:1053–1066.

Wallrabe, H., and A. Periasamy. 2005. Imaging protein molecules using FRET and FLIM microscopy. *Curr. Opin. Biotechnol.* 16:19–27.

Woehlke, G., A.K. Ruby, C.L. Hart, B. Ly, N. Hom-Booher, and R.D. Vale. 1997. Microtubule interaction site of the kinesin motor. *Cell*. 90:207–216.

Zal, T., and N.R. Gascoigne. 2004. Photobleaching-corrected FRET efficiency imaging of live cells. *Biophys. J.* 86:3923–3939.